

Thermal Hall conductivity of electron-doped cuprates: Electrons and phonons

Marie-Eve Boulanger^{§,1} Lu Chen^{§,1,*} Vincent Oliviero,² David Vignolles,² Gaël Grissonnanche,¹ Kejun Xu,^{3,4,5} Zhi-Xun Shen,^{3,4,5} Cyril Proust,² Jordan Baglo,^{1,†} and Louis Taillefer^{1,6,‡}

¹*Institut quantique, Département de physique & RQMP,
Université de Sherbrooke, Sherbrooke, Québec, Canada*

²*LNCMI-EMFL, CNRS UPR3228, Univ. Grenoble Alpes,
Univ. Toulouse, INSA-T, Grenoble and Toulouse, France*

³*Geballe Laboratory for Advanced Materials, Stanford University, Stanford, California, USA*

⁴*Stanford Institute for Materials and Energy Sciences,
SLAC National Accelerator Laboratory, Menlo Park, California, USA*

⁵*Departments of Physics and Applied Physics, Stanford University, Stanford, California, USA*

⁶*Canadian Institute for Advanced Research, Toronto, Ontario, Canada*

(Dated: October 25, 2023)

It has recently become clear that phonons generate a sizable thermal Hall effect in cuprates, whether they are undoped, electron-doped or hole-doped (inside the pseudogap phase). At higher doping, where cuprates are reasonably good metals, mobile electrons also generate a thermal Hall effect, the thermal equivalent of the standard electrical Hall effect. Here we show that in the cleanest crystals of the electron-doped cuprate $\text{Nd}_{2-x}\text{Ce}_x\text{CuO}_4$, at high doping, the phonon and electron contributions to the thermal Hall conductivity κ_{xy} are of comparable magnitude, but of opposite sign. In samples of lower quality, phonons dominate κ_{xy} , resulting in a negative κ_{xy} at all temperatures. The fact that the negative phononic κ_{xy} in the metallic state is similar in magnitude and temperature dependence to that found in the insulating state at lower doping rules out any mechanism based on skew scattering of phonons off charged impurities, since a local charge should be screened in the metallic regime. The phononic κ_{xy} is found to persist over the entire doping range where antiferromagnetic correlations are known to be significant, suggesting that such correlations may play a role in generating the phonon thermal Hall effect in electron-doped cuprates. If the same mechanism is also at play in hole-doped cuprates, the presence of a phononic κ_{xy} below (and only below) the critical doping p^* would be evidence that spin correlations are a property of the pseudogap phase.

PACS numbers: Valid PACS appear here

I. INTRODUCTION

The discovery of a large negative thermal Hall conductivity κ_{xy} in hole-doped cuprates [1], persisting down to zero doping ($p = 0$), in the Mott insulating phase [2], revealed a new and fascinating facet of cuprate high- T_c superconductors. This negative κ_{xy} , now attributed to phonons [2, 3], is a new experimental signature of the enigmatic pseudogap phase of cuprates, as it disappears above the critical doping p^* that marks the end of that phase. However, the microscopic mechanism that makes phonons in cuprates acquire a handedness in a magnetic field remains unknown. A number of theoretical proposals have recently been made, including a coupling of phonons to magnons [4] or spinons [5, 6], to collective fluctuations [7], and to a state of loop-current order with the appropriate symmetries [8], or the scattering of phonons by impurities or defects [9–12]. It is still unclear which of these mechanisms, if any, is appropriate for cuprates.

A recent study of electron-doped cuprates [13] showed that the negative thermal Hall conductivity in cuprates

is also present on the other side of the phase diagram. As a function of doping, the negative κ_{xy} signal is observed from the insulating antiferromagnetic phase at $x = 0$ all the way up to $x = 0.17$, in the metallic phase above optimal doping. And here also, this negative κ_{xy} was shown to be carried by phonons.

Now, in the metallic phase, electrons are also expected to generate a thermal Hall signal, due to the Lorentz force. In this study, we show that in our cleanest crystals of the electron-doped cuprate $\text{Nd}_{2-x}\text{Ce}_x\text{CuO}_4$ (NCCO), electrons and phonons make comparable contributions to the thermal Hall conductivity in the metallic state at high doping, but with opposite sign. The electronic contribution is large and positive, as expected from the Wiedemann-Franz law and the known electrical Hall conductivity σ_{xy} . The negative phononic contribution is similar in magnitude and temperature dependence to that found at lower doping, including $x = 0$ [13]. This shows that the phonon thermal Hall conductivity of cuprates is independent of whether the host material is an insulator or a metal. This rules out any mechanism based on the skew scattering of phonons off charged impurities, such as oxygen vacancies, as these local charges should be screened very effectively by mobile electrons in a highly conductive metallic state.

To further characterize our samples, we have looked for

[§]M.-E. B. and L. C. contributed equally to this work.

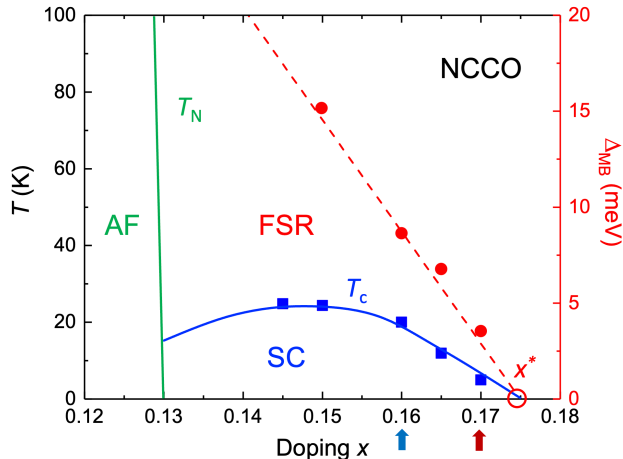


FIG. 1: Temperature-doping phase diagram of the electron-doped cuprate NCCO. The antiferromagnetic phase (AF) is bounded by the Néel temperature T_N (solid green line) and the superconducting phase (SC) by the zero-field critical temperature T_c (blue squares) [14]. The magnetic breakdown gap Δ_{MB} (red circles) obtained from quantum oscillations is a measure of how strongly the Fermi surface of NCCO is reconstructed [14]. The doping dependence of Δ_{MB} yields a critical doping $x^* = 0.175$ (open red circle) above which the Fermi surface is not reconstructed. The solid blue line and red dashed line are guides to the eye. In our study, we investigated two samples of NCCO, with nominal concentrations $x = 0.16$ (blue arrow) and $x = 0.17$ (red arrow).

quantum oscillations. The presence of a low frequency in our cleanest sample with $x = 0.16$ shows that the Fermi surface is reconstructed, clear evidence for the presence of significant antiferromagnetic correlations. We speculate that these correlations may play a role in generating the phonon thermal Hall signal in electron-doped cuprates, and possibly also in the pseudogap phase of hole-doped cuprates.

II. METHODS

A. Samples

Single crystals of $\text{Nd}_{2-x}\text{Ce}_x\text{CuO}_4$ with nominal concentrations $x = 0.16$ and 0.17 were grown by the traveling-solvent floating-zone method in O_2 and annealed in flowing argon for 48 hours at 900°C . Both samples have a doping such that they lie in the superconducting / metallic regime of the phase diagram (Fig. 1). The superconducting transition temperature in zero field, defined by the onset of the drop in magnetization, is $T_c = 23.5$ K and 20.0 K for $x = 0.16$ and 0.17 , respectively. For the transport measurements, crystals were cut into rectangular platelets with dimensions (length between contacts \times width \times thickness, in μm) $620 \times 660 \times 90$ ($x = 0.16$, sample 1), $1114 \times 1080 \times 185$ ($x = 0.16$, sam-

ple 2) and $1000 \times 1050 \times 80$ ($x = 0.17$). Contacts were made using silver epoxy, diffused at 500°C under oxygen for 1 h. The magnetic field was applied perpendicular to the CuO_2 planes. A field of $H = 15$ T is large enough to suppress superconductivity down to $T \rightarrow 0$ in both samples [15]. From the same mother crystals, another pair of NCCO samples were prepared, with $x = 0.16$ and $x = 0.17$, for the tunnel diode oscillator (TDO) measurements. The dimensions of these samples (in μm) are $730 \times 220 \times 100$ ($x = 0.16$) and $440 \times 300 \times 50$ ($x = 0.17$).

Note that it is difficult to achieve good enough electrical contacts on NCCO crystals to achieve a measurement of the in-plane electrical resistivity ρ_a that is free of c -axis current contamination in this highly 2D material. For this reason, we have turned to measurements of the thermal conductivity κ_{xx} down to very low temperature to access the residual resistivity ρ_0 of our samples. Heat transport does not suffer from c -axis contamination.

B. Thermal transport measurements

The thermal conductivity κ_{xx} is measured by applying a heat current J_x along the x axis of the sample (longest direction), which generates a longitudinal temperature difference $\Delta T_x = T^+ - T^-$. The thermal conductivity κ_{xx} is given by

$$\kappa_{xx} = \frac{J_x}{\Delta T_x} \left(\frac{L}{wt} \right), \quad (1)$$

where w is the sample width, t its thickness and L the distance between T^+ and T^- . When a magnetic field is applied perpendicular to the heat current ($H \perp J_x$) (*i.e.* parallel to z), a transverse temperature difference ΔT_y can develop along the y axis. The thermal Hall conductivity κ_{xy} is then given by

$$\kappa_{xy} = -\kappa_{yy} \left(\frac{\Delta T_y}{\Delta T_x} \right) \left(\frac{L}{w} \right), \quad (2)$$

after antisymmetrization, *i.e.* $\Delta T_y(H) = [\Delta T_y(T, +H) - \Delta T_y(T, -H)]/2$. Since NCCO is a tetragonal system, we can take $\kappa_{yy} = \kappa_{xx}$. The error bar on κ_{xx} and κ_{xy} is roughly $\pm 15\%$ for each, coming mostly from the uncertainty on sample dimensions and geometric factors.

We use a steady-state method to measure both thermal conductivity κ_{xx} and thermal Hall conductivity κ_{xy} . The data are taken while changing temperature in discrete steps at a fixed magnetic field. The thermal gradient along the sample is provided by a resistive heater connected to one end of the sample. The other end of the sample is glued to a copper block with silver paint which acts as a heat sink. Below 3 K, the longitudinal temperature difference ΔT_x is measured in a dilution refrigerator down to 50 mK, using two RuO_2 thermometers calibrated *in situ* as a function of temperature and magnetic field. The transverse temperature difference ΔT_y

is measured using two RuO₂ thermometers connected to opposite sides of the sample. Above 3 K, ΔT_x and ΔT_y are measured in a standard variable temperature insert (VTI) system up to 100 K, using type-E thermocouples, known to have a weak magnetic field dependence. More details of the technique can be found in refs. 2, 3, 16.

C. TDO measurements

Quantum oscillations were detected using a tunnel diode oscillator method (TDO) in a magnetic field up to 85 T down to 1.8 K. The sample is placed on a compensated spiral coil of a self-resonating LC circuit operating around 20 MHz. The circuit is driven by a tunnel diode polarized in its negative resistance region of the current-voltage characteristic. The driving system (tunnel diode + capacitor) is separated from the TDO coil by a 1.25-meter-long coaxial cable and the magnetic field was applied perpendicular to the CuO₂ planes.

In a TDO measurement, variations in the electrical resistance of the sample change the coil inductance through skin depth [17] resulting in a shift in the TDO resonance frequency. By measuring this shift, one can detect Shubnikov-de Haas (SdH) oscillations.

III. RESULTS

A. Thermal transport

In Fig. 2(a), we display the thermal Hall conductivity of our two main samples, $x = 0.16$ (sample 1) and $x = 0.17$, plotted as κ_{xy}/H vs T below 100 K (down to 3 K), for three different magnetic fields H . At $H = 15$ T, we find that κ_{xy} is negative at all temperatures for the sample with $x = 0.17$ (blue squares), whereas it is positive at all temperatures for the sample with $x = 0.16$. The negative κ_{xy} is similar to that found at lower doping [13], down to $x = 0$, and it is due to phonons. The positive κ_{xy} is due to electrons.

There is a contribution of phonons and electrons in both samples, but the electronic contribution is much larger in the sample with $x = 0.16$. This is confirmed by performing measurements down to very low temperature. In Fig. 3(b), we report our κ_{xy} data at $H = 15$ T taken below 4 K, plotted as κ_{xy}/T vs T . The fact that κ_{xy}/T is constant below 4 K shows that it is entirely coming from transport by fermions, *i.e.* electrons. Indeed, the contribution of phonons to κ_{xy} in cuprates is negligible below 4 K [2]. We see that this (positive) electronic contribution is 10 times larger in the sample with $x = 0.16$, as reflected in the residual linear term κ_{xy}^0/T , obtained by extrapolating κ_{xy}/T to $T = 0$ (dashed lines), seen to equal to 175 ± 30 mW/K²m for $x = 0.16$ and 17.5 ± 10 mW/K²m for $x = 0.17$.

As previously reported in NCCO samples with lower dopings [13], the temperature dependence of κ_{xy}/H vs T

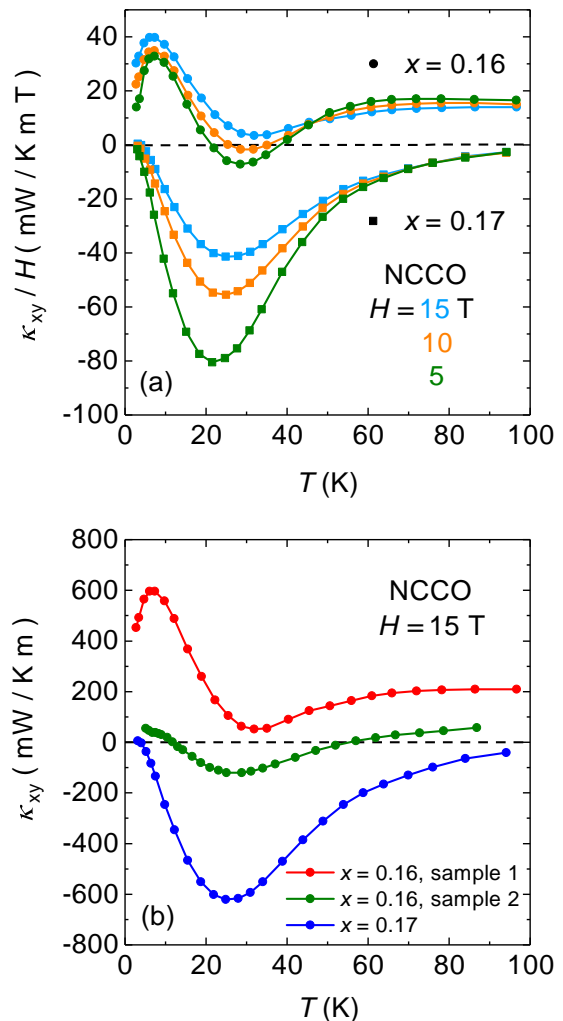


FIG. 2: (a) Field dependence of the thermal Hall conductivity for NCCO $x = 0.16$ (circles) and $x = 0.17$ (squares) at $H = 5$ T (green), 10 T (orange) and 15 T (blue), plotted as κ_{xy}/H vs T . We can observe two behaviours: the negative thermal Hall conductivity of phonons (very clear in the sample with $x = 0.17$ and also visible in the sample with $x = 0.16$) and the positive electronic thermal Hall conductivity (visible only in the sample with $x = 0.16$). (b) Thermal Hall conductivity for NCCO $x = 0.16$ and $x = 0.17$ at $H = 15$ T, plotted as κ_{xy} vs T . $x = 0.16$ sample 1 is cleaner than sample 2, results in a larger positive electronic contribution.

in the $x = 0.16$ sample shows different sign and temperature dependence. In $x = 0.16$ sample, the thermal Hall conductivity is positive at $H = 15$ T over all temperature range, being maximal around 10 K before aiming for a finite residual value as T goes to 0. We attribute this positive signal to the electronic contribution which we believe is larger in the $x = 0.16$ sample.

It is also worth to notice that while $H = 15$ T is strong enough to fully suppress superconductivity in both samples, $H = 5$ T is not. However, the fact that κ_{xy} follows the same temperature dependence at both $H = 15$ T and 5 T indicates that superconductivity has little to no

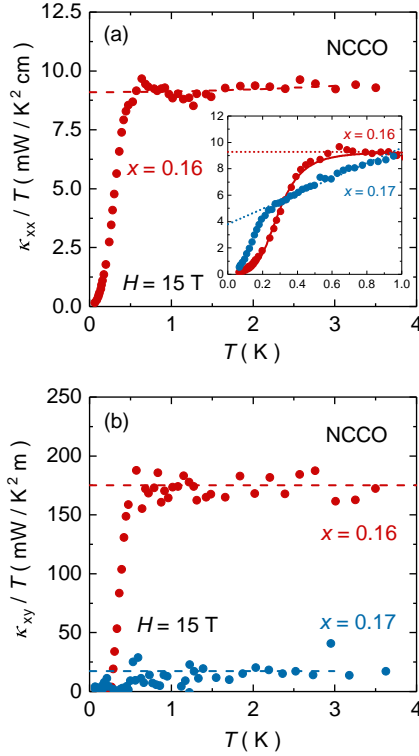


FIG. 3: (a) Thermal conductivity for NCCO $x = 0.16$ at $H = 15$ T, plotted as κ_{xx}/T vs T . The dashed line is a linear fit to extract the residual term in the form $\kappa_{xx}/T = \beta T^2 + \frac{\kappa_0}{T}$, with $\beta = 0.03$ mW/K⁴cm and $\kappa_{xx}^0/T = 9.1 \pm 0.1$ mW/K²cm. A ρ_0 of 2.7 ± 0.1 $\mu\Omega$ cm can be estimated by the WF law from the residual linear term κ_{xx}^0/T . Inset: Thermal conductivity for NCCO $x = 0.16$ (red) and $x = 0.17$ (blue) at $H = 15$ T, plotted as κ_{xx}/T vs T , below 1 K. We can observe a large downturn in κ_{xx}/T as $T \rightarrow 0$, characteristic of the electron-phonon decoupling. The red solid line is a fit using eqn (3), which gives a decoupling temperature of $T_{dec} = 291$ mK. Dotted lines are linear fit that gives a residual linear term of $\kappa_{xx}^0/T = 4.0 \pm 0.1$ mW/K²cm and ρ_0 of 6.1 ± 0.1 $\mu\Omega$ cm for $x = 0.17$ sample. (b) Thermal Hall conductivity for NCCO $x = 0.16$ and $x = 0.17$ at $H = 15$ T plotted as κ_{xy}/T vs T . We can extract a residual linear term of $\kappa_{xy}^0/T = 175 \pm 20$ mW/K²m for $x = 0.16$ and $\kappa_{xy}^0/T = 17.5 \pm 10$ mW/K²m for $x = 0.17$.

effect on the thermal Hall response on both samples.

The thermal Hall conductivity is also measured in NCCO $x = 0.16$ sample 2 which is dirtier than sample 1 (as shown in Fig. 2 (b)). We find that the overall κ_{xy} signal is more negative in sample 2 compared to sample 1, which indicates that the positive electronic contribution is larger in a cleaner sample due to less scattering of electrons by impurities.

The positive electronic contribution of κ_{xy} is larger in NCCO $x = 0.16$ than $x = 0.17$ is simply due to the fact that $x = 0.16$ sample is cleaner. This can be verified by making a direct comparison on their thermal conductivity data at low temperature. Fig. 3 (a) shows the longitudinal thermal conductivity, plotted as κ_{xx}/T vs T , at low

temperature down to $T \rightarrow 0$. Since both samples are in the metallic region of the phase diagram, a residual linear term is expected. By applying a linear fit (inset of Fig. 3 (a), dashed lines), we obtain $\kappa_0/T = 9.1$ mW/K²cm for $x = 0.16$ and $\kappa_0/T = 4.0$ mW/K²cm for $x = 0.17$. Using the Wiedemann-Franz (WF) law, we can estimate a $\rho_0 = 2.7 \pm 0.1$ $\mu\Omega$ cm for the former and $\rho_0 = 6.1 \pm 0.1$ $\mu\Omega$ cm for the later. There's roughly a factor of 2.25 between the two ρ_0 s, which clearly shows that the $x = 0.16$ sample is cleaner than the $x = 0.17$ sample.

As we can observe in Fig 3, there is a large downturn in both κ_{xx} and κ_{xy} below $T \sim 500$ mK. A similar downturn has been observed in $\text{Pr}_{2-x}\text{Ce}_x\text{CuO}_4$ (PCCO) at $T \sim 300$ mK, which was attributed to the thermal decoupling between electrons and phonons at low temperature [18]. The decoupling temperature T_{dec} can be extracted by fitting the κ_{xx}/T curve using the following formula:

$$\kappa_{xx}/T = \alpha \frac{1}{1 + \frac{r}{1+r(T/T_{dec})^{n-1}}} + \beta T^2 \quad (3)$$

in which α , β , r , n and T_D are all fitting parameters [18]. In the inset of Fig. 3 (a), the red solid line denotes the thermal decoupling fit using eqn. (3), which gives a decoupling temperature of $T_{dec} = 291$ mK. This value is higher than $T_{dec} = 160$ mK obtained in PCCO [18].

Fig. 4 (a) shows the thermal conductivity for NCCO $x = 0.16$ (red) and $x = 0.17$ (blue), plotted as κ_{xx}/T vs T , at $H = 15$ T for the whole T range. The data are a combination of the low temperature measurement (obtained in a dilution fridge, circles) and the high temperature measurement (obtained in a standard VTI, triangles). In the same figure, we also plot an estimate of the expected electronic contribution (dashed lines), calculated using the Wiedemann-Franz law: $\kappa_{xx}^e/T = L_0\sigma_{xx}$ with $\sigma_{xx} = \rho_{xx}/[\rho_{xx}^2 + \rho_{xy}^2]$. For those estimation, we use the published data of $\rho_{xx}(T)$ of PCCO at $x = 0.17$ in ref. [15], but with the calculated value of ρ_0 obtained from thermal conductivity. For $\rho_{xy}(T)$, we use the published data of PCCO at $x = 0.17$ in ref. [19], with $\rho_{xy}(T) \equiv R_H(T) \times H$. From those estimation, we can already infer that, even though the phonons are the main heat carriers in thermal transport, the electronic contribution is larger in $x = 0.16$ than in $x = 0.17$.

Fig. 4(b) shows the electronic thermal Hall conductivity κ_{xy}^e/T vs T in NCCO $x = 0.16$ (blue solid line) with the estimated thermal Hall conductivity of the electrons $L_0\sigma_{xy}$ (red dashed line) obtained using the WF law. κ_{xy} of NCCO $x = 0.17$ is dominated by the negative phononic contribution. Thus, κ_{xy}^e in NCCO $x = 0.16$ can be obtained by subtracting the κ_{xy} of $x = 0.17$ from $x = 0.16$, assuming the phononic κ_{xy} is similar in NCCO $x = 0.16$ and $x = 0.17$. The red dashed line represents the upper limit of the estimated electronic contribution $L_0\sigma_{xy}$ by WF law, with $\sigma_{xy} = \rho_{xy}/[\rho_{xx}^2 + \rho_{xy}^2]$. $L_0\sigma_{xy}$ is calculated by using a temperature independent Hall coefficient R_H and a temperature dependent $\rho_{xx}(T)$ data of PCCO at $x = 0.17$ [15], but adjusted with a $\rho_0 = 2.7$ $\mu\Omega$ cm. To match the value of $\kappa_{xy}^e/T = 175 \pm 20$

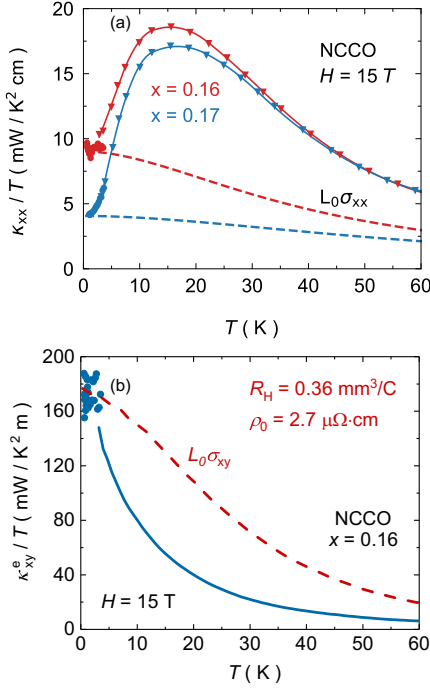


FIG. 4: (a) Thermal conductivity for NCCO $x = 0.16$ (red) and $x = 0.17$ (blue) plotted as κ_{xx}/T vs T at $H = 15 \text{ T}$. Dashed lines are the expected electronic contribution obtained from WF law (see text). (b) The electronic part of thermal Hall conductivity plotted as κ_{xy}^e/T vs T for NCCO $x = 0.16$ (red) at $H = 15 \text{ T}$. κ_{xy}^e is obtained by subtracting the κ_{xy} of $x = 0.17$ from $x = 0.16$, assuming the phononic κ_{xy} is the same in $x = 0.16$ and $x = 0.17$. The red dashed line represents the estimated electronic contribution $L_0\sigma_{xy}$ by WF law. $L_0\sigma_{xy}$ is calculated by using a temperature independent Hall coefficient R_H and a temperature dependent $\rho_{xx}(T)$ data of PCCO at $x = 0.17$ [15], but adjusted with a $\rho_0 = 2.7 \mu\Omega\text{cm}$. To match the value of $\kappa_{xy}^e/T = 175 \pm 20 \text{ mW}/\text{K}^2$ at $T \rightarrow 0$, we get a Hall coefficient of $R_H = 0.36 \text{ mm}^3/\text{C}$, which is half of the expected value ($\sim 0.7 \text{ mm}^3/\text{C}$) in PCCO at $x = 0.17$ [19].

mW/K^2 at $T \rightarrow 0$, we get a Hall coefficient of $R_H = 0.36 \text{ mm}^3/\text{C}$, which is half of the expected value ($\sim 0.7 \text{ mm}^3/\text{C}$) in PCCO at $x = 0.17$ [19]. Judging by the doping dependence of R_H in PCCO $x = 0.17$, the estimated R_H in NCCO $x = 0.16$ confirms that the doping level is lower but close to the Fermi surface reconstruction point $x^* = 0.175$.

B. Quantum oscillations

Another smoking gun evidence that the NCCO $x = 0.16$ sample is cleaner than $x = 0.17$ is from the quantum oscillation measurements. By performing the TDO measurements in both $x = 0.16$ and $x = 0.17$ samples up to 85 T , we are able to observe quantum oscillation

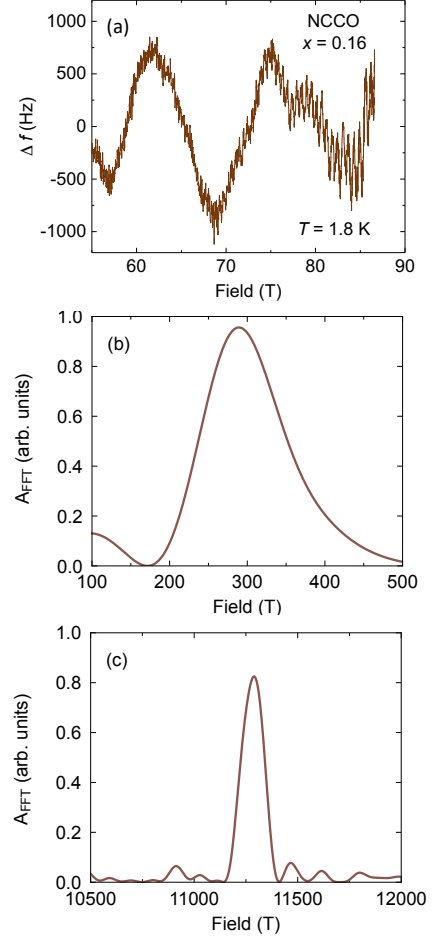


FIG. 5: Quantum oscillation pattern observed by TDO measurement. (a) The oscillatory part of the TDO signal after removing a smooth background taken in the $x = 0.16$ sample at $T = 1.8 \text{ K}$. (b) - (c) Discrete Fourier analysis of the data, showing two peaks at frequencies $F_1 = (290 \pm 20) \text{ T}$ and $F_2 = (11300 \pm 100) \text{ T}$.

signals in the $x = 0.16$ sample but not in the $x = 0.17$ sample, which indicates that the $x = 0.16$ sample is indeed cleaner than the $x = 0.17$ sample.

The quantum oscillation data after subtracting a smooth background taken in the $x = 0.16$ sample are shown in Fig. 5 (a). After applying a discrete Fourier analysis, we can extract two frequencies $F_1 = (290 \pm 20) \text{ T}$ (Fig. 5 (b)) and $F_2 = (11300 \pm 100) \text{ T}$ (Fig. 5 (c)). Close to $x^* = 0.175$, the FS undergoes a reconstruction due to the AF ordering, which results in electron-like and hole-like FSs. The low frequency oscillations come from the small hole pocket, while the emergence of the higher frequency can be explained by the magnetic breakdown between the hole- and electron-like FSs, which was previously reported in another study [14].

From the Lifshitz-Kosevich (LK) theory, the temperature and magnetic field dependence of the oscillation amplitude are determined by the product of the thermal damping factor R_T and the Dingle damping factor R_D ,

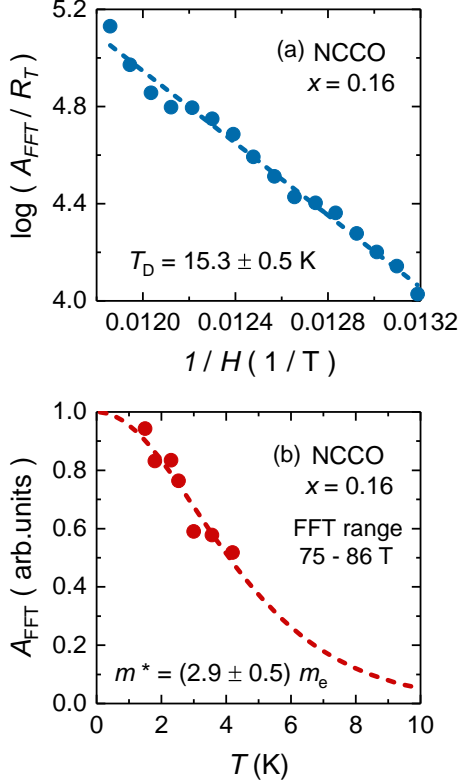


FIG. 6: (a) Dingle plot of the oscillation amplitude of the 11.3 kT peak, at $T = 1.5$ K, giving the Dingle temperature $T_D = 15.3 \pm 0.5$ K. Dashed line is the fit to the Dingle factor. (b) The temperature dependence of the FFT amplitude of the 11.3 kT peak, normalized by the $T \rightarrow 0$ limit. Fitting the oscillatory amplitude to the LK formula (dashed line) gives the effective mass $m = (2.9 \pm 0.5)m_e$ for the higher frequency.

defined as

$$R_T = \frac{\alpha T m^*}{B \sinh(\alpha T m^*/B)}, \quad (4)$$

$$R_D = \exp[-\alpha T_D m^*/B], \quad (5)$$

where the effective mass $m = m^*m_e$ and the Dingle temperature $T_D = \hbar/2\pi k_B \tau$. τ is the scattering rate, k_B is the Boltzmann constant, m_e is the bare electron mass and $\alpha = 2\pi^2 k_B m_e / e \hbar = 14.69$ T/K. We can then fit the temperature dependence of the normalized damping factor (Fig. 6 (b)) to obtain an effective mass of $m = (2.9 \pm 0.5)m_e$ for the high frequency. Fig. 6 (a) shows the field dependence of the oscillation amplitude. A linear fit yields a Dingle temperature of $T_D = (15.3 \pm 0.5)$ K. Both the extracted effective mass and Dingle temperature are consistent with previous results when comparing samples with similar T_c (and not the nominal doping), which results in a doping level slightly lower than $x = 0.16$ [20].

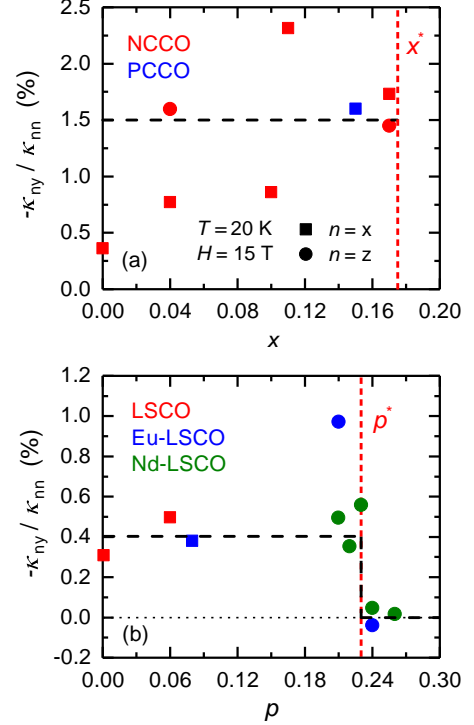


FIG. 7: The ratio between thermal Hall conductivity and thermal conductivity as a function of doping, plotted as $-\kappa_{ny}/\kappa_{nn}$ vs. *doping*, taken at $T = 20$ K and $H = 15$ T in (a) electron-doped cuprates and (b) hole-doped cuprates. $n = x(z)$ denotes the heat current is applied along the $a(c)$ axis. Data for hole-doped cuprates are taken from Ref. [21]. Data for electron-doped cuprates are taken from Ref. [13]. For hole-doped cuprates, to obtain the phononic part of the thermal Hall signal, $n = x$ data are used for the three lowest dopings ($p \leq 0.08$), where the electronic thermal conductivity is negligible and the signal is dominated by phonons. For higher dopings ($p > 0.08$), $n = z$ data are used. The ratio becomes zero outside the pseudogap phase ($p > 0.23$). Data are plotted in the same way for the electron-doped cuprates.

IV. DISCUSSION

The main finding of this study is the positive thermal Hall conductivity for NCCO $x = 0.16$ sample in the metallic state, compared to a large negative κ_{xy} signal in the $x = 0.17$ at $H = 15$ T. Knowing, from a previous study [13], that the κ_{xy} observed at $x = 0.17$ is dominated by phonons, we can propose two distinct mechanisms for κ_{xy} in NCCO $x = 0.16$. The positive contribution of κ_{xy} comes from electrons, which is partially compensated by the negative contribution of phonons. The electronic κ_{xy} is larger in $x = 0.16$ sample is simply due to the fact that $x = 0.16$ sample is cleaner than $x = 0.17$, which can be verified by a smaller residual resistivity ρ_0 in $x = 0.16$ and the absence of QOs in $x = 0.17$. In the same doping level of $x = 0.16$, the electronic contribution is also larger in a cleaner sample (as shown in Fig. 2(b)), due to the fact of less scattering of electrons by

impurities.

Combining these results with a previous study [13], we find that the large negative electron contribution have similar magnitude and temperature dependence at all doping levels in electron-doped cuprates NCCO (as shown in Fig. 7(a)). This observation indicates that the mechanism behind the phonon thermal Hall effect in e-doped cuprates is similar among all doping levels, regardless of whether the system is an insulator or metal. What is intriguing here is, electrons and phonons make comparable contributions to the thermal Hall conductivity in the metallic state at $x = 0.16$, but with opposite sign. This puts strong limits on possible mechanisms behind the phonon thermal Hall effect and rules out any mechanism based on the skew scattering of phonons off charged impurities [10], such as oxygen vacancies, as these local charges should be screened very effectively by mobile electrons in a highly conductive metallic state.

So what makes phonons chiral in cuprates? One possible explanation is the skew scattering of phonons by impurities imbedded within an AF environment [12]. Both the extracted Hall coefficient and QOs measurements in NCCO $x = 0.16$ sample confirms its proximity to the FS reconstruction point, where short-range AF correlations are still prominent. A large negative phonon contribution, similar in magnitude and temperature dependence, persists from the AF ordered Mott insulating state all the way up to the metallic state close to x^* , is consistent with a scenario of AF ordering playing a key role in the phonon thermal Hall effect.

It is worth to be noted that a similar κ_{xy} consists of both negative phononic contribution and positive electronic contribution has also been observed in the hole-doped cuprate $p = 0.20$ $\text{La}_{1.6-x}\text{Nd}_{0.4}\text{Sr}_x\text{CuO}_4$ sample [1], like in the case of $x = 0.16$ NCCO. As can be seen in Fig. 7 (b), a negative phonon contribution, also similar in magnitude and temperature dependence, persists from the Mott insulating state all the way up to the pseudogap phase below p^* . This similar behavior of the phonon thermal Hall effect in hole-doped cuprates and electron-doped cuprates indicates that the same mechanism involving AF correlations could potentially also explain the phonon κ_{xy} in hole doped cuprates, as has been suggested by a very recent study of impurity-induced phonon thermal Hall effect in the AF phase of Sr_2IrO_4 [22].

V. SUMMARY

We have measured the thermal conductivity κ_{xx} and the thermal Hall conductivity κ_{xy} of the electron-doped cuprate NCCO at dopings $x = 0.16$ and $x = 0.17$. In the $x = 0.16$ sample, we observe two distinct but comparable channels for thermal Hall conductivity in the metallic state. The positive channel is contributed by electrons and the sign is consistent with the prediction from the electrical Hall conductivity σ_{xy} . The negative channel is contributed by phonons and it persists up to $x = 0.17$ with a similar magnitude and temperature dependence to that found at lower doping. The fact that the negative phononic contribution is comparable regardless of the system being an insulator or a metal indicates that its origin is unlikely to come from skew scattering of phonons off charged impurities, since such a mechanism should depend strongly on the screening from mobile electrons. The fact that the negative phonon thermal Hall effect persists from the AF ordered phase all the way up to x^* , where short-range AF correlations are still present, is consistent with spin texture playing a role in the underlying mechanism for the phonon thermal Hall effect. This type of mechanism, whereby phonons are scattered by spin texture or defects embedded in a magnetic order, could also apply to hole-doped cuprates inside their pseudogap phase (below the critical doping p^*).

VI. ACKNOWLEDGMENTS

We thank S. Fortier for his assistance with the experiments. L.T. acknowledges support from the Canadian Institute for Advanced Research and funding from the Institut Quantique, the Natural Sciences and Engineering Research Council of Canada (Grant No, PIN:123817), the Fonds de Recherche du Québec - Nature et Technologies, the Canada Foundation for Innovation, and a Canada Research Chair. This research was undertaken thanks in part to funding from the Canada First Research Excellence Fund. Z-X.S. acknowledges the support of the U.S. Department of Energy, Office of Science, Office of Basic Energy Sciences, Division of Material Sciences and Engineering, under contract DE-AC02-76SF00515.

* Electronic address: lu.chen@usherbrooke.ca

† Electronic address: jordan.baglo@usherbrooke.ca

‡ Electronic address: louis.taillefer@usherbrooke.ca

¹ G. Grissonnanche, A. Legros, S. Badoux, E. Lefrançois, M. L. V. Zako, F. Laliberté, A. Gourgout, J.-S. Zhou, S. Pyon, T. Takayama, et al., *Nature* **571**, 376–380 (2019).

² M.-E. Boulanger, G. Grissonnanche, S. Badoux, A. Allaire, E. Lefrançois, A. Legros, A. Gourgout, M. Dion, C. H. Wang, X. H. Chen, et al., *Nat. Commun* **11**, 5325 (2020).

³ G. Grissonnanche, S. Thériault, A. Gourgout, M.-E.

Boulanger, E. Lefrançois, A. Ataei, F. Laliberté, M. Dion, J.-S. Zhou, S. Pyon, et al., *Nat. Phys.* **16**, 1108 (2020).

⁴ M. Ye, L. Savary, and L. Balents, arXiv:2103.04223 (2021).

⁵ R. Samajdar, S. Chatterjee, S. Sachdev, and M. S. Scheurer, *Phys. Rev. B* **99**, 165126 (2019).

⁶ Y. Zhang, Y. Teng, R. Samajdar, S. Sachdev, and M. S. Scheurer, *Phys. Rev. B* **104**, 035103 (2021).

⁷ L. Mangeolle, L. Balents, and L. Savary, *Phys. Rev. B* **106**, 245139 (2022).

⁸ C. M. Varma, *Phys. Rev. B* **102**, 075113 (2020).

- ⁹ H. Guo and S. Sachdev, Phys. Rev. B **103**, 205115 (2021).
- ¹⁰ B. Flebus and A. H. MacDonald, Phys. Rev. B **105**, L220301 (2022).
- ¹¹ X.-Q. Sun, J.-Y. Chen, and S. A. Kivelson, Phys. Rev. B **106**, 144111 (2022).
- ¹² H. Guo, D. G. Joshi, and S. Sachdev, Proc. Natl. Acad. Sci. U.S.A. **119**, (46) e2215141119 (2022).
- ¹³ M.-E. Boulanger, G. Grissonnanche, E. Lefrançois, A. Gourgout, K.-J. Xu, Z.-X. Shen, R. L. Greene, and L. Taillefer, Phys. Rev. B **105**, 115101 (2022).
- ¹⁴ T. Helm, M. V. Kartsovnik, I. Sheikin, M. Bartkowiak, F. Wolff-Fabris, N. Bittner, W. Biberacher, M. Lambacher, A. Erb, J. Wosnitza, et al., Phys. Rev. Lett. **105**, 247002 (2010).
- ¹⁵ F. F. Tafti, F. Laliberté, M. Dion, J. Gaudet, P. Fournier, and L. Taillefer, Phys. Rev. B **90**, 024519 (2014).
- ¹⁶ G. Grissonnanche, F. Laliberté, S. Dufour-Beauséjour, M. Matusiak, S. Badoux, F. F. Tafti, B. Michon, A. Riopel, O. Cyr-Choinière, J. C. Baglo, et al., Phys. Rev. B **93**, 064513 (2016).
- ¹⁷ T. Coffey, Z. Bayindir, J. F. DeCarolis, M. Bennett, G. Esper, and C. C. Agosta, Rev Sci Instrum. **71**, 4600 (2000).
- ¹⁸ M. F. Smith, J. Paglione, M. B. Walker, and L. Taillefer, Phys. Rev. B **71**, 014506 (2005).
- ¹⁹ S. Charpentier, G. Roberge, S. Godin-Proulx, X. Béchamp-Laganière, K. D. Truong, P. Fournier, and P. Rauwel, Phys. Rev. B **81**, 104509 (2010).
- ²⁰ T. Helm, Ph.D. thesis, Technische Universität München, Munich (2013).
- ²¹ S. Thériault, Ph.D. thesis, Université de Sherbrooke, Sherbrooke (2022).
- ²² A. Ataei, G. Grissonnanche, M.-E. Boulanger, L. Chen, E. Lefrançois, V. Brouet, and L. Taillefer, arXiv:2302.03796 (2023).